Experimental and Numerical Analysis of Single Phase Flow in a micro T-junction

Pamela VOCALE[1], Giacomo PUCCETTI[2,*], Beatrice PULVIRENTI[2], Gian Luca MORINI[2]

* Corresponding author: Tel.: +39 051 2090540; Fax: +39 051 2090544; Email: giacomo.puccetti2@unibo.it
1 Department of Industrial Engineering, University of Parma, Italy
2 DIN –Laboratorio di Microfluidica, Alma Mater Studiorum Università di Bologna, Italy

Abstract In this work the fluid-dynamic behaviour of a micro T-junction has been investigated both numerically and experimentally for low Reynolds numbers (Re<14) with water as working fluid. The velocity profiles within the T-junction has been experimentally determined by using the micro Particle Image Velocimetry (μPIV). The experimental data have been compared with the numerical results obtained by means of a 3D model implemented in Comsol Multiphysics® environment for incompressible, isothermal, laminar flows with constant properties. The comparison between the experimental and the numerical data puts in evidence a perfect agreement among the results. In the central region of the T-junction where the velocity profiles of the inlet branches interact, the maximum difference is less than 5.8% for different flow rates imposed at the inlet (with the ratio 1:2) and less than 4.4% in the case of the same flow rate at the inlets (1:1). Since the estimated uncertainty of the experimental velocity is about 3%, the obtained result can be considered very good and it demonstrates that no significant scaling effects influences the liquid mixing for low Reynolds numbers (Re<14) and the behaviour of the micro T-junction can be considered as conventional. The detailed analysis of the velocity profile evolution within the central region of the mixer has allowed to determine where the fully developed laminar profile is reached (for instance 260 μm far from the centre of the T-junction when a maximum water flow rate of 8 ml/h is considered).

Keywords: Micro Flow, micro T -junction, microPIV, Microchannel.

1. Introduction

The recent years have seen a very fast growth of microfluidic miniaturized devices for research purposes and for industrial uses. Scaling down the characteristic size of the system from the macroscopic scale to the microscopic one, the physical laws governing the motion of fluids change due to the presence of scaling effects. As observed by Tabeling (2005), at the microscale, the superficial forces become more important than the volume forces. In this way, single-phase and two-phase flows through microdevices can show marked differences with respect to their well-known behaviour in conventional systems. For this reason, during the last years a large number of experimental and numerical studies have been conducted in order to verify the entity of the changes linked to the reduction of the size of the channels on the fluid-dynamic

rules and, with this aim, innovative experimental techniques which enable the analysis of the dynamic behaviour of fluids through microdevices without disturbing the same motion of fluid have been proposed, tested and developed (Sinton 2004).

One of the most important non-intrusive diagnostic techniques of the fluid velocity field within microchannels is the micro Particle Image Velocimetry (μPIV) presented by Santiago et al. (1998) and Meinhart et al. (1999). Starting from these two works, many research groups began to use and develop this technique until to make it the state of art of the diagnostic techniques for fluid flows within microchannels, for both single phase flows and multi-phase flows (Lindken et al. 2009, Steijn et al. 2007, Lee and Kim 2009, Bayraktar and Pidugu 2006). The original μPIV technique has been modified in the last years by introducing the use of infrared light, with the

advantage to be able to utilize microdevices made in silicon, as demonstrated by Liu et al. (2004), a high-speed C-MOS camera for the study of transient phenomena (Shinohara et al., 2004) or stereomicroscopy, used to capture µPIV images of the flow in a microchannel from two different angles in order to make a 3D reconstruction of the motion of a fluid within microchannels (Lindken et al. 2006). µPIV has been extensively used for the fluid dynamic characterization of micromixers, micro-manifolds, micro-separators. As an example, Hoffmann et al. (2005) have performed an experimental investigation of the mixing in a T-shaped micro mixer device, by using µPIV for determining the velocity field and µLIF technique for analysing the evolution of the concentration field in the region afterward the junction. The experimental results obtained by Hoffmann et al. underline that, despite laminar flow conditions, short diffusion lengths are achievable in microjunctions.

In this paper a deep analysis of the fluid-dynamic mixing mechanism activated in a micro T-junction in presence of laminar flows is presented by combining experimental results obtained using µPIV with numerical results obtained with Comsol. The comparison between the numerical and the experimental results presented in this paper demonstrates that it is possible to reach with µPIV a high quality reconstruction of the velocity profiles within the thin region afterward the junction in which the change of the velocity profile due to the merged flows is more pronounced. Within this region, experimental and numerical velocity profiles have been compared starting from the centre of the junction toward the direction of the outflow with steps of 10 µm in order to reconstruct the complete evolution of the laminar profile within the T-junction until the condition of fully developed flow is reached along the outflow branch.

2. Experimental set-up

2.1 µPIV apparatus

The lay-out of the experimental set-up is shown in Figure 1. µPIV is composed by a pulsed Nd:YAG ($\lambda = 532$ nm) monochromatic green laser *(NanoPIV, Litron Lasers)* (1, in Fig.1) able to emit two pulses with a duration of the order of 5 ns each one with a time delay between pulses variable from hundreds of nanoseconds to few seconds. The illumination light, through beam-forming optics (2), is delivered to the inverse microscope *(EclipseT2000, Nikon,* 3). The illumination light is reflected upward towards the objective lens by a dichroic antireflective coated mirror designed to reflect wavelength 532 nm and transmit 560 nm (4). A Nikon air immersion lens (5) with a numerical aperture $NA = 0.75$ and magnification $M = 20$ is used.

The T-junction used in these experimental tests is a commercial glass micro T-junction (*Translume, 6*) obtained as intersection of two straight microchannels of fused silica with a nominal squared cross-section with a side of 300 µm. Both microchannels are made by laser etching on a substrate of high quality fused silica and then bonded with the same material. The relative roughness of the inner walls declared by the manufacturer is less than 0.1%.

Pure water at ambient temperature has been used as working fluid. Fluorescent seeding (*Invitrogen)* is dispersed in the working fluid. The particle tracer presents a diameter of 1.0 µm, a density of $\rho_p = 1.05$ g/cm^3, orange coloration, a carboxylate coating. When illuminated with a green light ($\lambda = 532$ nm) these particles emit a radiation wavelength of 560 nm. The seeded working fluids are delivered to the T-junction with the help of two syringes (Hamilton Gastight #1010, 7) of 10.0 ml volume. A constant flow rate of seeded liquid flow can be imposed along the two inlet branches of the T-junction by means of two programmable syringe pumps (Harvard Apparatus PHD 4400, 8).

The light emitted by the seeding is collected by the microscope objective, and addressed to a sensitive large-format interline-transfer CCD camera *(Sensicam, PCO,* 9) which is used to record the position of the particles. The interline transfer feature of the CCD camera allows for two image frames to be recorded back-to-back to within a 500 ns

time delay. A Dantec synchronization unit (10), connected with the laser, the CCD camera and a computer (11), coordinates the light pulse and the acquisition of the images. The illumination intensity of the laser beam is set from a remote control (12).
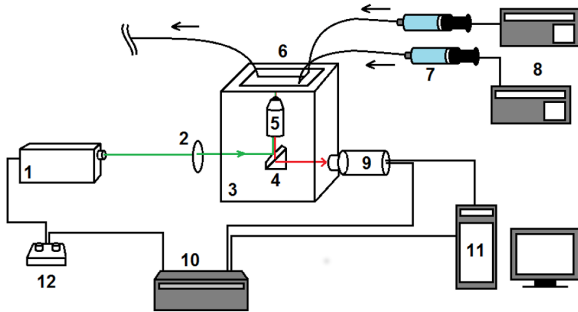

Fig. 1. Layout of the experimental set-up.

2.2 Imaging and post-processing

In order to improve the accuracy of the cross-correlation used for extracting the velocity values by the recorded images, 400 couples of images have been acquired for each experimental run. The post-processing of the recorded images returns the whole velocity field on the central plane of the T-junction as a vector map, similar to the velocity field shown in Fig.2. The vector map reported in Fig. 2 has been obtained after the average cross correlation of the 400 recorded image couples by adopting an interrogation window of 64x64 pixel with an overlap of 50%. In this way the velocity field is obtained with a resolution area of 10 µm x 10 µm.
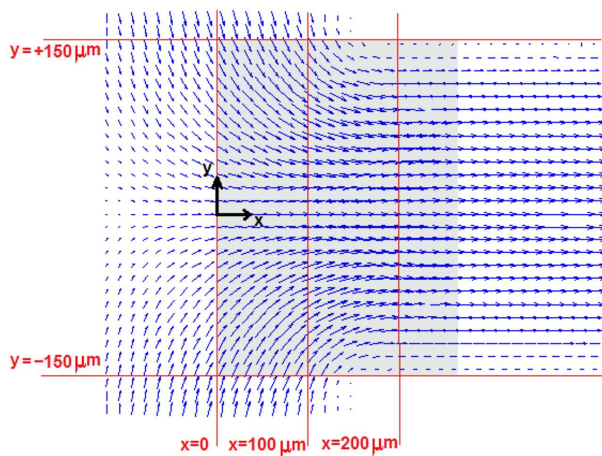

Fig. 2. Experimental vector map of the velocity field.

The velocity obtained by the µPIV images, expressed in pixels per unit time, have

been translated in m/s by using the following definition:

$$u(x, y) = \frac{s_{pix} L_p}{\Delta t L_{pix}} \tag{1}$$

where $u(x,y)$ is the fluid velocity, s_{pix} is the displacement in pixels of the interrogation window obtained by cross-correlation between two consecutive images, Δt is the time delay between the couple of images, L_p is the width in meters of the channel's plan under investigation and L_{pix} is the width of the same plan in pixels. Eq.(1) underlines that it is important to obtain an accurate measure of the width of the channel in order to obtain an accurate evaluation of the velocity field.

From the whole velocity field, the velocity profiles for a fixed value of the axial coordinate x (see the red lines and the coordinate system shown in Fig. 2) have been extracted in order to follow the evolution of the velocity profile from the centre of the T-junction (x=0 in Fig. 2) up to the axial coordinate in correspondence of which a fully developed laminar velocity profile is established along the outflow branch (grey area in Fig. 2). In this way it is possible to measure the distance from the centre of the T-junction employed to reach the fully developed region as a function of the mass flow rates of water imposed on the inlet branches of the T-junction.

According to Silva et al. (2009), the velocity uncertainty has been estimated to be of the order of 3%.

3. Numerical analysis

3.1 Governing equations

The dynamic behaviour of two laminar flows of the same fluid (water in this case) introduced in the micro T-junction has been also studied numerically. A Cartesian coordinate system (x,y,z), is introduced with the origin in the centre of the T-junction, as shown in Fig. 2. Assuming that the fluid is Newtonian, incompressible, isothermal and with constant physical properties, the classical continuity and Navier-Stokes equations can be written as follows:

$$\frac{\partial u_x}{\partial x} + \frac{\partial u_y}{\partial y} + \frac{\partial u_z}{\partial z} = 0 \tag{2}$$

$$\rho \left(u_x \frac{\partial u_x}{\partial x} + u_y \frac{\partial u_x}{\partial y} + u_z \frac{\partial u_x}{\partial z} \right) = -\frac{\partial p}{\partial x} +$$
$$+ \mu \left(\frac{\partial^2 u_x}{\partial x^2} + \frac{\partial^2 u_x}{\partial y^2} + \frac{\partial^2 u_x}{\partial z^2} \right) \tag{3}$$

$$\rho \left(u_x \frac{\partial u_y}{\partial x} + u_y \frac{\partial u_y}{\partial y} + u_z \frac{\partial u_y}{\partial z} \right) = -\frac{\partial p}{\partial y} +$$
$$+ \mu \left(\frac{\partial^2 u_y}{\partial x^2} + \frac{\partial^2 u_y}{\partial y^2} + \frac{\partial^2 u_y}{\partial z^2} \right) \tag{4}$$

$$\rho \left(u_x \frac{\partial u_z}{\partial x} + u_y \frac{\partial u_z}{\partial y} + u_z \frac{\partial u_z}{\partial z} \right) = -\frac{\partial p}{\partial z} +$$
$$+ \mu \left(\frac{\partial^2 u_z}{\partial x^2} + \frac{\partial^2 u_z}{\partial y^2} + \frac{\partial^2 u_z}{\partial z^2} \right) \tag{5}$$

where u_x, u_y and u_z are the scalar components of the velocity, ρ and μ are the fluid density (997 kg/m^3 in this case) and dynamic viscosity (8.57e^{-4} Pa s in this case), respectively, and p denotes the pressure.

The fluid has a uniform inlet velocity, at both inlet branches of the T-junction, therefore the inflow boundary conditions are:

$$u_x = 0 \quad u_y = W_1 \quad u_z = 0 \quad at \ the \ inlet \ 1 \tag{6}$$

$$u_x = 0 \quad u_y = W_2 \quad u_z = 0 \quad at \ the \ inlet \ 2 \tag{7}$$

in which W_1 and W_2 are the average fluid velocity at the inlets. These two values of inlet velocity are easily calculated by the volumetric flow rates imposed during the experimental tests at the inlet branches of the T-junction if the cross section area of the branches is known. At the walls, the no-slip boundary condition has been imposed.

For the purpose of the present study, Eqs. (2) – (5) linked to their boundary conditions have been solved within the Comsol Multiphysics® environment.

To analyse the grid independence of the numerical results, several mesh sizes have been considered. The grid resolution has been analysed by monitoring the convergence of the local values of velocity. For each analysed mesh size the *NRMS error*, defined in Eq. (8), has been calculated on the whole cross-section of the channel in the fully developed region of the outflow branch of the T-junction.

$$NRMS = \frac{\sqrt{\frac{1}{n} \sum_{i=1}^{n} \left(u_i - u_{i,ref} \right)^2}}{\left(u_{ref,max} - u_{ref,min} \right)} \tag{8}$$

In Fig. 3 the *NRMS error* as a function of the number of elements (*N*) is depicted. In here presented results, the *NRMS error* has been calculated by considering 69 points (i.e. *n*=69) and the velocity profile obtained adopting the finest mesh (i.e. *N*=1200000) as reference.
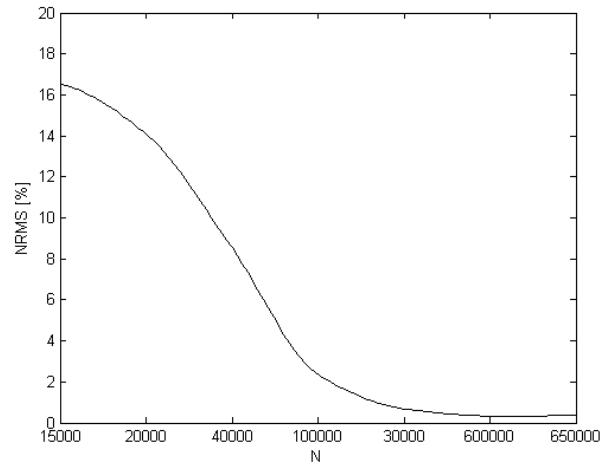

Fig. 3. *NRMS error* as a function of the number of finite elements adopted in the mesh (*N*).

By observing Fig. 3 it can be noticed that for a number of finite elements (*N*) higher than 600000 the *NRMS error* tends to become zero which means that the numerical values of the velocity become independent on the grid size. Therefore the numerical simulations have been performed by considering a number of finite elements higher than 600000 for each numerical run.

4. Results and discussion

As above described, the manufacturer declared that the branches of the T-junction are squared with a side of 300 μm. Adopting the geometry declared by the manufacturer for the post-processing of the velocity data, it has been made a comparison between: 1) the experimental velocity profile obtained for an axial position (x=1.5 mm) along the outlet branch of the T-junction where the velocity

profile is fully developed; 2) the numerical data obtained by Comsol; 3) the analytical laminar velocity profile obtained adopting the solution for rectangular channels proposed by Morini (2000).

The comparison between the numerical results obtained considering a grid with more than 600000 elements, and the analytical results shows a perfect agreement, as depicted in Fig. 4 where the two velocity profiles are essentially overlapped.

Moreover, in Fig. 4 the experimental velocity profile obtained by μPIV considering the cross section of the microchannel as declared by the manufacturer is shown. The *rRMS error (e)* between experimental data and analytical results, defined in Eq. (9), is about 14% and the maximum of the error occurs in the centre of the channel, as it can be noticed by observing Fig. 4.

$$e = \sqrt{\frac{1}{M} \sum_{m=1}^{M} \left(\frac{u_m - v_m}{v_m} \right)^2} \qquad (9)$$

In Eq. (9) u_m is the experimental velocity and v_m is the value of the theoretical velocity calculated by solving N-S equations in the same position of the experimental velocity.
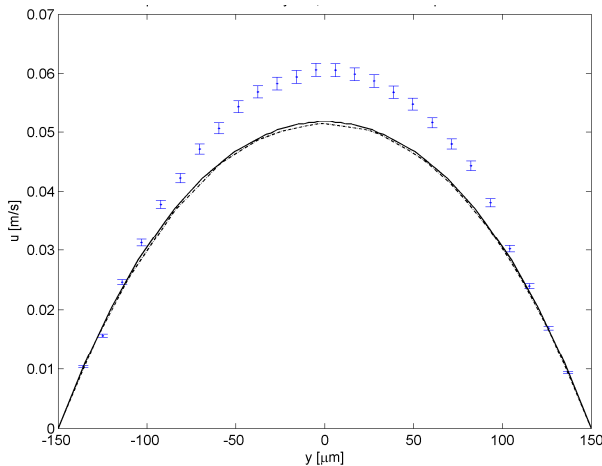

Fig. 4. Comparison between analytical solution (continuous line), numerical solution (dotted line) and experimental data (blue points with error bar) in fully developed region (*i.e.* outlet branch of the T-junction).

Values of *rRMS* error larger than 10% suggest that the geometry of the channel has not been correctly determined, as observed by Puccetti et al. (2014). This result was anticipated by the mismatch observed experimentally between the depth of the channels declared by the manufacturer (300 μm) and the measured depth of the microchannel (265 μm). This result cannot be considered a surprise because in many cases a mismatch between the geometry declared by the microdevices manufacturers and the real dimensions, is found (see Morini et al. 2011). Therefore, it is always suggested to test accurately the geometry of microdevices before analysing the obtained results (Puccetti et al. 2014).

Moreover, from the accurate analysis of the microscopy images it can inferred that the lateral sides of the microchannels are not perfectly vertical but the cross section appears to be slightly trapezoidal with apex angles of about 88°. This finding is coherent with the results obtained by Puccetti et al. (2014) during the tests of similar glass microchannels, made by the same manufacturer; their experimental results have been confirmed by a destructive SEM analysis.

The experimental evidence on the real cross section geometry of the microchannels has been used to numerically model the T-junction; the squared microchannels have been replaced with trapezoidal microchannels having the apex angles of 88°, the maximum width of 300 μm and the depth of 265 μm. Adopting this geometry, the disagreement between the numerical and experimental profiles in the fully developed region, along the outlet branch of the T-junction, disappears; this finding confirm that the microchannels geometry has been correctly determined.

For a more complete investigation of the fluid-dynamic mechanism of recombination of the velocity profile within the T-junction, three different sets of imposed water flow rate have been tested. A reference flow-rate of 4 ml/h for both the inlets has been chosen. Later, for one inlet, the flow-rate is kept constant at the reference value and for the other one, the flow-rate is firstly halved and then doubled respect to the reference value. For all the cases, the Reynolds number (*Re)* is always below the value of 14.

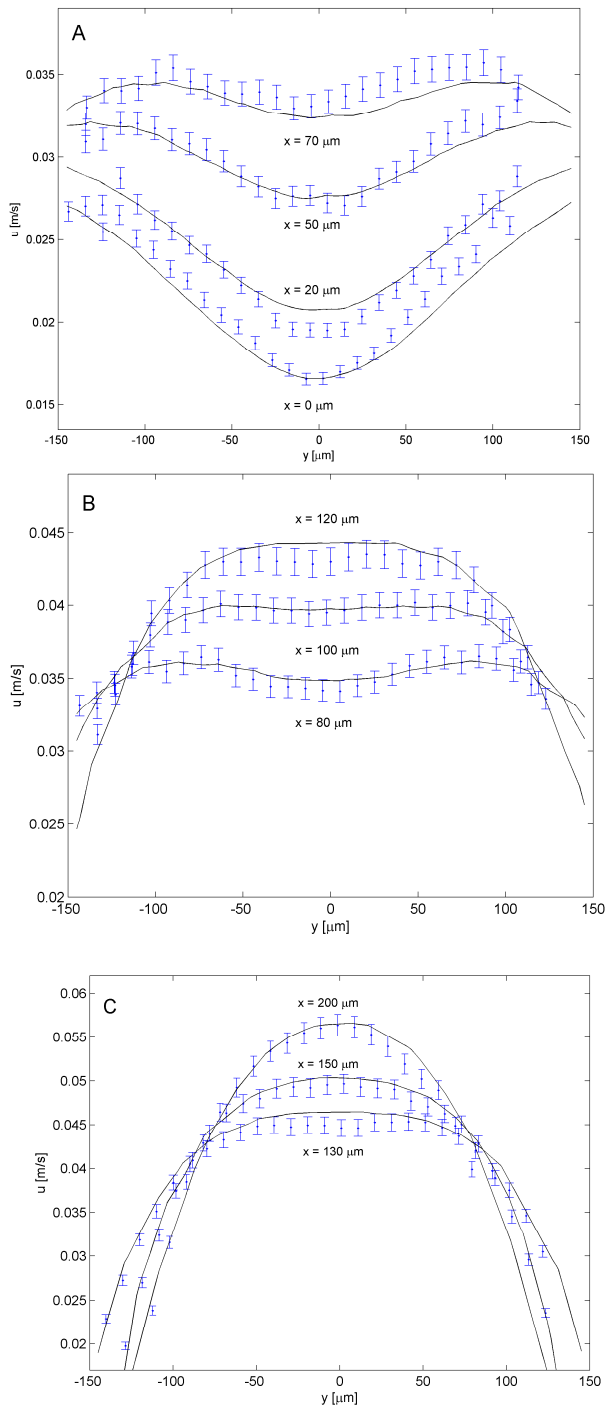Figure 5 shows the comparison between

Fig. 5. Comparison between experimental data (blue points with error bar, error bars ± 3 %) and numerical solution (continuous line) for reference flow rates (**4 ml/h** and **4 ml/h**) at x = 0, 20 μm, 50 μm, 70 μm (A), x = 80 μm, 100 μm, 120 μm (B) and at x = 130 μm, 150 μm and 200 μm (C).

experimental data and numerical results for fixed axial position ranging from x=0 (centre of the T-junction) up to x=200 μm along the intersection for the two streams into the junction, for two imposed flow rates equal

to 4 ml/h at the inlet branches of the T-junction (reference flow-rates).

In order to study the mechanism of laminar recombination of the velocity profiles within the T-mixer starting from x=0 (i.e. the origin of the axes shown in Fig. 2), the velocity profiles on different sections, perpendicular to the outlet stream direction, with a step of 10 μm from each other, have been analysed. As mentioned before, the velocity profiles have been acquired on the horizontal central plane of the sample, where the velocity reaches the maximum value.

The evolution of the velocity profiles depicted in Fig. 5 shows that the velocity profiles linked to the two inlet flows at the centre of the T-junction (x=0) are still completely separated, as it can be observed in Fig. 6. At the centre of the junction (x=y=0) the velocity is near to zero which means that there exist a stagnant fluid region from x=-150 μm and x=0, as confirmed by Fig. 2. The interaction between the two streams increases the value of the velocity at the centre of the T-junction (y=0) when x increases; at x=70 μm (keeping y=0) the velocity value is twice with respect to the one at x=0 and y=0 and the velocity profile tends to become parabolic. A flat velocity profile can be observed in the centre part of the outlet channel from x=100 μm up to x=130 μm.

The local developed laminar profile is finally reached at 260 μm of distance from the centre of the T-junction.
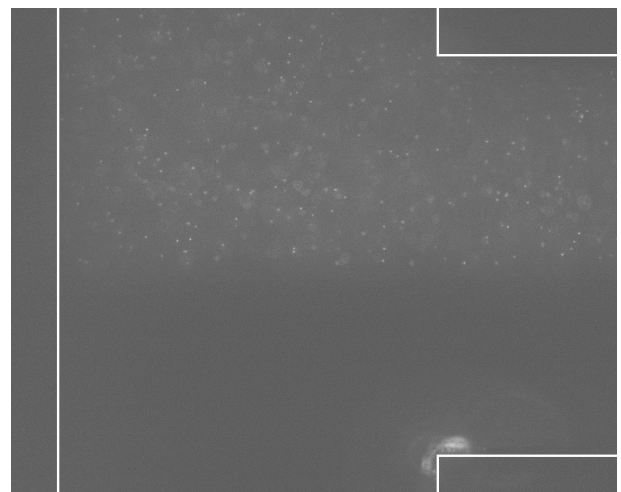

Fig. 6. Image of fluorescent particles after filtering for reference flow rates (**4 ml/h** and **4 ml/h**).
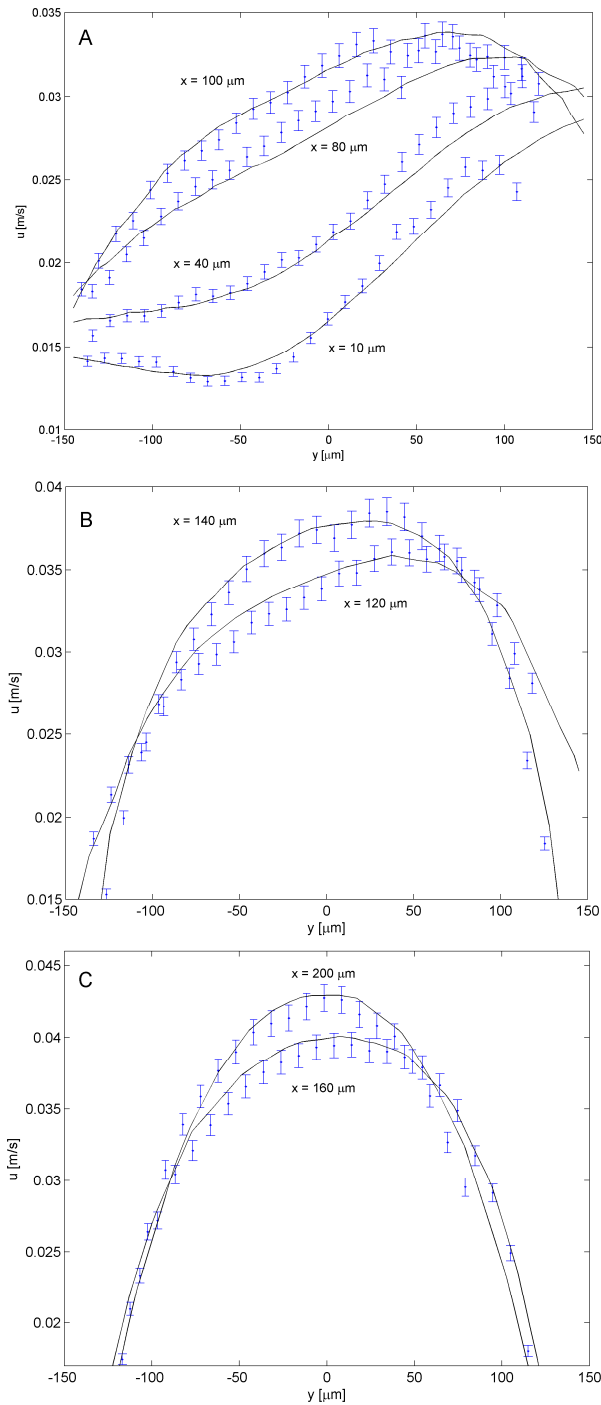
Fig. 7. Comparison between experimental data (blue points with error bar, error bars ± 3 %) and numerical solution (continuous line) for a halved flow rate of one branch (**2 ml/h** and **4 ml/h**) at x = 10 μm, 40 μm, 80 μm, 100 μm (A), x = 120 μm, 140 μm (B) and at x = 160 μm and 200 μm (C).

In Fig. 7 the same comparison have been made for a halved flow rate imposed on one inlet branch of the T-junction. In this case the different flow rates at the two inlet branches breaks the symmetry of the velocity profile with respect to the y direction.

The stagnant region close to the centre of the T-junction is shifted to the inlet branch with a low flow rate of water. The symmetry of the velocity profile is recovered slowly along the outlet branch and the profile becomes fully developed for *x* smaller than 260 μm.

In Figures 5 and 7 the uncertainty over velocity module has been plotted by means of an error bar linked to each experimental data.

It is interesting to observe that the experimental velocity profiles are in very good agreement with the prediction of the numerical model along the whole region of the T-junction investigated.

In order to quantify the agreement between the numerical predictions and the experimental data the *rRMS e* value obtained by applying Eq.(9) between experimental data and numerical results has been calculated for each profile as a function of the axial coordinate (x) and of the imposed flow rates at the inlets. The value of the error *e* found for each profile is shown in Tab.1.

Tab. 1. Value of rRMS error *e* [%]

x position	Flow rate [ml/h]		
[μm]	4 and 4	2 and 4	8 and 4
0	4.4	5.8	5.6
20	4.2	3.4	5.7
40	2.4	3.5	3.3
60	2.6	3.4	3.5
80	1.3	3.5	3.6
100	1.2	2.8	3.6
120	1.9	2.9	3.9
140	3.6	5.4	5.7
160	1.3	4.7	5.4

By analysing the data reported in Tab. 1 it can be pointed out that the maximum *rRMS error* is 5.8%; however in most of analysed sections, the *rRMS error* is less than 4%. This demonstrates the high accuracy of the results obtained by using μPIV in this T-junction analysis.

Regarding to the analysis on the different condition of flow rate, is possible to see how for the reference condition of flow rate (*i.e.*

when the two flow rate are the same) the lowest values of *rRMS error* have been observed. For this condition, indeed, the *rRMS* is about 2.8% and never goes over the value of 5%. For the other two conditions of flow-rate the error *e* is higher than the reference one and sometimes goes over the 5%. Moreover, the trend of the data acquired with a halved flow-rate of one supply branch is very close to the one obtained by acquiring the data with a doubled flow-rate of one supply branch, as must be theoretically.

5. Conclusions

The analysis of merging laminar flows in a micro T-junction has been carried out, adopting both experimental technique (μPIV) and numerical approach (Comsol).

The comparison among the results, within the central region of the mixer, shows a perfect agreement between the experimental and the numerical results. In most of analysed velocity profiles the difference is less than 4%.

Moreover the detailed analysis of the velocity profile evolution has highlighted that the fully developed laminar profile is reached 240 μm, 260 μm or 310 μm far from the centre of the micro T-junction, for maximum flow rate equal to 6 ml, 8 ml or 12 ml, respectively.

Finally, as indirect result, it has been demonstrated the μPIV measurements can be employed in order to check the geometry of a microdevice without resorting to destructive tests and in the same time of the microdevice test.

Acknowledgements

References

Bayraktar, T., Pidugu, S. B., 2006. Characterization of liquid flows in microfluidic systems. Int. J. Heat Mass Transfer, 49, 815–824.

Hoffmann, M., Schlüter, M., Räbiger, N., 2005. Experimental investigation of liquid-liquid mixing in T-shaped micro-mixers using μ-LIF and μ-PIV.

Chem. Eng. Sci., 61, 2968-2976.

Lee, S. J., Kim, S., 2009. Advanced particle-based velocimetry techniques for microscale flows. Microfluid Nanofluid, 6, 577–588.

Lindken, R., Westerweel, J., Wienke, B., 2006. Stereoscopic micro particle image velocimetry. Exp. in Fluids. 41, 161-171.

Lindken, R., Rossi, M., Große, S., Westerweel, J., 2009. Micro-Particle Image Velocimetry (μPIV): Recent developments, applications, and guidelines. Lab on a Chip, 9, 2551-2567.

Liu, D., Garimella, S. V., Wereley, S. T., 2004. Infrared micro-particle image Velocimetry in silicon-based microdevices. Exp in Fluids, 38, 385-392.

Meinhart, C. D., Wereley, S. T., Santiago, J. G., 1999. PIV measurements of microchannel flow. Exp in Fluids, 27, 414-419.

Morini, G. L., 2000. Analytical determination of the temperature distribution and Nusselt numbers in rectangular ducts with constant axial heat flux. Int J Heat Mass Transfer, 43, 741-755.

Morini, G.L., Yang, Y., Chalabi H., Lorenzini, M., 2011. A Critical review of the measurement techniques for the analysis of gas microflows through microchannels, Exp Therm and Fluid Sci, 35, 6, 849-865.

Puccetti, G., Pulvirenti, B., Morini, G.L., 2014. Use of μPIV technique for an indirect determination of the microchannel cross-section passage geometry. Journal of Physics: Conference Series 501 (1), 012027.

Puccetti, G., Pulvirenti, B., Morini, G.L., 2014. Experimental Determination of the2D Velocity Laminar Profile in Glass Microchannel Using μPIV, Energy Procedia, 45, 538-547.

Santiago, J: G., Wereley, C. D., Meinhart, C. D., Beebe, D. J., Adrian R. J., 1998. A particle image velocimetry system for microfluidics. Exp. in Fluids, 25, 316-319.

Silva, G., Leal, N., Semiao, V., 2009. Determination of microchannels geometric parameters using micro-PIV, Chem. Eng. research and design, 87, 298-306.

Shinohara, K., Sugii, Y., Aota, A., Hibara, A., Tokeshi, M., Kitamori, T., Okamoto, K., 2004. High-speed micro-PIV measurements of transient flow in microfluidics devices. Meas. Sci. Technol, 15, 1965-1970.

Steijn, V., Kreutzer, M. T., Kleijn, C. R., 2007. μ-PIV study of the formation of segmented flow in microfluidic T-junctions. Chem. Eng. Sci., 62, 7505-7514.

Tabeling, P., 2005. Introduction to Microfluidics. Oxford University Press, USA.